Confidence intervals ($P<0.05$) were calculated according to the method of a previous report [11].

RT-PCR and direct sequencing

Total RNA was isolated from the skin of five-week-old animals using ISOGEN (NIPPON GENE, Tokyo, Japan). RT-PCR and direct sequencing of the PCR product was carried out as described previously [15]. Rat *Hr* cDNA was amplified using the following eight primer sets: rHr-01&02 CACCTGTGGAAGGCTGCT and ACAGGGTCACTCTTGGGATG; rHr-03&04 AGGGACTACGCTGGAAGGAA and CCCAAACGTTACCGAGAGTG; rHr-05&06 GCAGGCAGCAGAATCTTTG and TCCTGTGGATGTCTCTGGTG; rHr-07&08 ACTCAAGAGGGCAGGCAGT and GGTGTTGAAGAGTCCGTGGT; rHr-09&10 CTTCCATCAACAAGGGCCTA and CTGGGCTCTCTGTGGAGTCT; rHr-11&12 GGTCAGCAGAAGGAACCAAC and TTCCAGAATGCTGTGCTGTC; rHr-13&14 GACTTAGCCTGTGGGGAATG and CTCCAAGGTTCCTGCTCCAG; rHr-15&16 GTCTCCAGGTAGCCAGACCA and GTTCCCTGCTTGTACCCAAA. The PCR products overlapped each other and spanned the entire 3,624 bp *Hr* coding sequence (CDS).

Morphological analysis

Dorsal and ventral skin samples were collected from *krh/krh* and *krh/+* littermates at two, nine and seventeen weeks of age. Mouse anti-cytokeratin (AE1/AE3, Dako Japan, Tokyo, Japan) was used for immunohistochemical analysis of the skin samples. Bound antibody was detected using horseradish peroxidase conjugated anti-mouse antibody (Histofine Simplestain MAX-PO; Nichirei, Tokyo, Japan) and 3,3'-diaminobenzidine as a chromogen (Vector Laboratories, Burlingame, CA, USA). To detect lipids, frozen sections were made from specimens that had been fixed with formalin and they were stained with Oil red O.

Organ samples of the heart, lungs, liver, pancreas, kidneys, spleen, lymph nodes, salivary glands, lacrimal glands, thyroid gland, adrenal glands, small and large intestines, and knee and foot joints, were collected from three *krh/krh* rats and three F344 rats at 40 weeks of age. They were fixed using 10% neutral buffered formalin, embedded in paraffin, cut at 4 μm in thickness, and then stained with hematoxylin and eosin (HE). To study glomerular lesions, periodic acid-Schiff (PAS) or periodic acid-methenamine-silver (PAM) staining was employed. For immunofluorescence studies, kidney samples were frozen in 22-oxacalcitriol compound (Miles Inc., Elkhart, IN, USA).

Electron microscopy

Perfusion fixation through the left ventricle was conducted with 4% paraformaldehyde in 0.1 M phosphate buffer (PB). Kidneys that had been excised were stored in 2% paraformaldehyde and 2.5% glutaraldehyde in 0.1 M PB. They were fixed with 2% osmic acid for 2 h and embedded in epoxy resin. Ultra-thin sections were double-stained with uranyl acetate and lead citrate and examined using a Hitachi H-7500 electron microscope (Hitachi, Tokyo, Japan).

Urine protein measurement

To collect urine, six male *krh/krh* rats and six F344/NSlc (+/+) rats, 40 weeks of age, were caged individually in metabolic chambers after they had been orally loaded with physiological saline at 2.5 ml/100 g body weight. Six-hour urine samples were collected and their volumes, and protein concentrations were determined. Statistical differences were determined using the Mann-Whitney U test.

Results

krh/krh rat hair loss phenotype and skin morphology

For the *krh/krh* rats, hair loss first occurred around the nose around 2 weeks after birth and extended gradually from the anterior to the posterior of the body (Fig. 1A and 1B). At around four months of age they had wrinkled skin, cystic hair canals and long curved nails.

Through histopathological analysis, markedly dilated hair follicles were observed. These cystic follicles contained a lot of keratin debris (Fig. 1C), and they stained positive for cytokeratin (Fig. 1D). The cysts were lined by a thin layer of squamous epithelium and an easily identifiable granular cell layer. The sebaceous glands that surrounded the dilated cysts were hyperplastic. Staining with Oil red O revealed that a large amount of lipids was present in the lumen of each cyst and on the

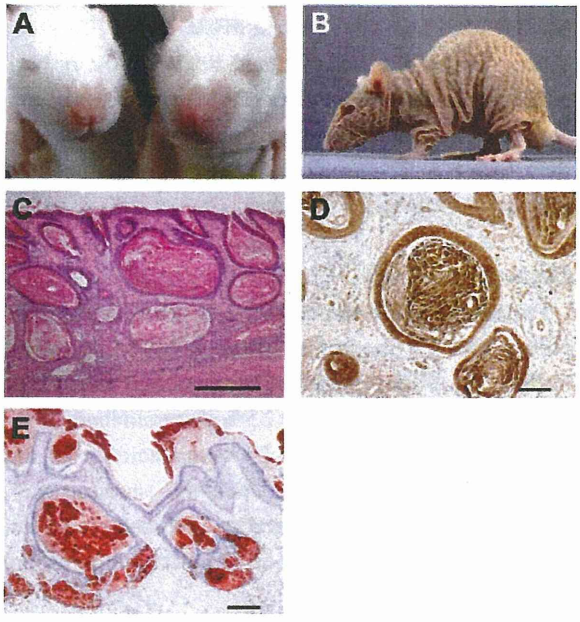

Fig. 1. Phenotypic and morphological characteristics of the Kyoto rhino rat. A: Right; a 2-week-old *krh/krh* rat with characteristic hair loss on the snout. Left; a littermate *krh/+* rat. B: Rhinocerotic appearance of a 10-week-old *krh/krh* rat. C: Histopathology of 9-week-old *krh/krh* rat skin. HE staining. Bar=500 μm. D: IHC of keratin of a 9-week-old *krh/krh* rat. Bar=100 μm. E: Oil Red O staining of a 17-week-old *krh/krh* rat. Bar=100 μm.

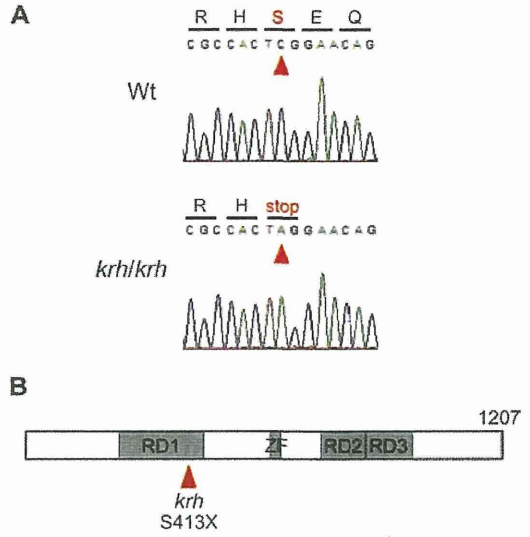

Fig. 2. Identification of the *krh* mutation. A: Results of direct sequencing of *Hr* cDNA of wild-type and *krh/krh* rats. The C-to-A nonsense mutation at position 1,238 is indicated by red arrowheads. The substitution produces a stop codon at amino acid residue 413 of protein HR. B: Schematic of the conserved domains in rat protein HR. RD1, RD2, and RD3 are used to denote the repression domains and ZF is used to denote the zinc-finger domain. The mutation site Ser413Ter is noted with a red arrowhead.

surface of the epidermis (Fig. 1E). These findings are indicators that the *krh/krh* skin and hair phenotypes are similar to those of *rh* at the *Hr* locus of the laboratory mouse [7].

krh is an Hr nonsense mutation

Hr on Chr 15 was believed to be the best candidate for *krh* and therefore the genotype of the backcross progeny was determined using genetic markers for Chr 15. We obtained 12 *krh/krh* and 8 *krh/+* rats from the (BN/SsNSlc × F344-*krh/krh*)F_1 × F344-*krh/krh* backcross. A significant linkage relationship was observed between *krh* and *D15Rat10* (42.7 Mb) with no recombination (χ^2=21.6, P<0.01), which is indicative that *krh* is located <13.9 cM away from *D15Rat10* with 95% probability [11]. *krh* was expected to span from 28.8 Mb to 56.6 Mb of Chr 15, within which the *Hr* locus (50.9 Mb) was mapped (RGSC v3.4).

Sequencing analyses of *Hr* cDNA obtained from *krh/krh* skin samples revealed that adenine (A) had been substituted for cytosine (C) at nucleotide position 1,238 from the start of the CDS (c. 1,238 C>A). This substitution resulted in a stop codon at amino acid 413 of the HR protein (p. Ser413Ter) (Fig. 2A). The truncated HR protein lacked a zinc-finger domain, a part of repression domain (RD) 1, and all of RD2 and RD3 (Fig. 2B). We characterized *krh* as an *Hr* nonsense mutation and called it Hr^{krh}.

Focal glomerulosclerosis and proteinuria in the aged Hr^{krh}/Hr^{krh} rat

Histopathological examinations of organs that were taken from Hr^{krh}/Hr^{krh} rats at 40 weeks of age were performed. No lesions that are associated with autoimmune diseases were observed, however, prominent glomerular lesions were noted in the kidneys of the Hr^{krh}/Hr^{krh} rats. These lesions were focal lesions that had collapsed glomeruli and protein exudates in Bowman capsule and the renal tubules (Fig. 3A and 3C), and segmental prolifera-

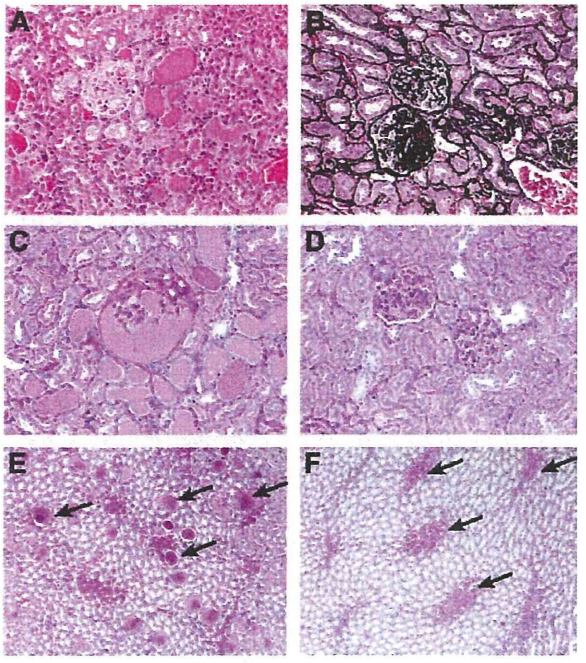

Fig. 3. Focal glomerular sclerotic lesions in 40-week-old Hr^{krh}/Hr^{krh} rat. Note that a collapsed glomerulus with protein exudates in Bowman's capsule and protein casts in renal tubules (A, C), and segmental proliferation of mesangial matrices (B, D) were seen. In the renal medulla, protein casts were notable in the collecting tubules (E) (arrows), but those in a wild-type F344 rat (+/+) were limited only to Henle's loop (F) (arrows). A: HE; B: PAM; C–F: PAS staining.

tion of the mesangial matrices (Fig. 3B and 3D). There was no inflammatory cell infiltration into the glomeruli and interstitium. In the renal medulla, protein casts were notably present in the collecting tubules (Fig. 3E). For the wild-type rats, protein casts were only observed in Henle's loop, possibly due to the effects of aging (Fig. 3F). These findings are indicators that the lesions that were observed in the F344-Hr^{krh}/Hr^{krh} rat were caused by focal glomerulosclerosis (FGS). Moreover, Hr^{krh}/Hr^{krh} rats at 40 weeks of age had proteinuria. The Hr^{krh} homozygous rats had significantly higher urine protein concentrations than age-matched wild-type rats: 152 ± 80.3 vs. 51.0 ± 38.5 mg/dl, (average ± SD), $P<0.02$ (Fig. 4).

From the electron microscopic observations, the segmental glomerular sclerotic lesions were characterized as having proliferating mesangial matrices (Fig. 5A). The proliferation was associated with the dendritic pro-

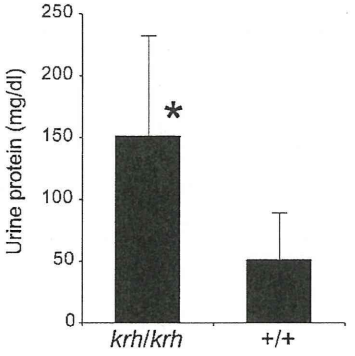

Fig. 4. Urine protein concentrations of Hr^{krh}/Hr^{krh} rats and wild-type F344 (+/+) rats. The Hr^{krh} homozygous rats had significantly higher urine protein concentrations than age-matched wild-type rats. Bars indicate standard deviation. *: $P<0.02$.

cesses of mesangial cells and on rare occasions with dense deposits in the mesangial regions. Foot process fusion was often observed in these glomeruli (Fig. 5B).

Discussion

The *krh* mutation was identified as an *Hr* nonsense mutation and therefore called Hr^{krh}. Protein HR is a nuclear receptor co-repressor for multiple nuclear receptors, such as the thyroid hormone receptor and the vitamin D receptor [23]. In the hair follicle (HF), the absence of functioning HR proteins results in the synthesis of premature and dysregulated catagen. This results in the destruction of the normal HF architecture and abrogates the HF's ability to cycle [20]. The Hr^{krh}/Hr^{krh} rat has cystic hair follicles and suffers from a premature hair cycle (Fig. 1). The truncated HR protein that is encoded by the Hr^{krh} nonsense mutation is caused by a lack of functional domains which play important roles in regulating target genes [23]. Additionally, the mutation may cause nonsense mediated mRNA decay. Therefore, it is likely that Hr^{krh} may be a loss-of-function mutation. In humans, *HR* mutations are associated with congenital alopecia, such as ALUNC and APL [2, 4, 9]. Because rats are suitably sized for handling and manipulating [5, 21], the Hr^{krh}/Hr^{krh} rat may be a useful animal model for developing therapies for these human diseases.

The aged Hr^{krh} homozygous rat has FGS which is as-

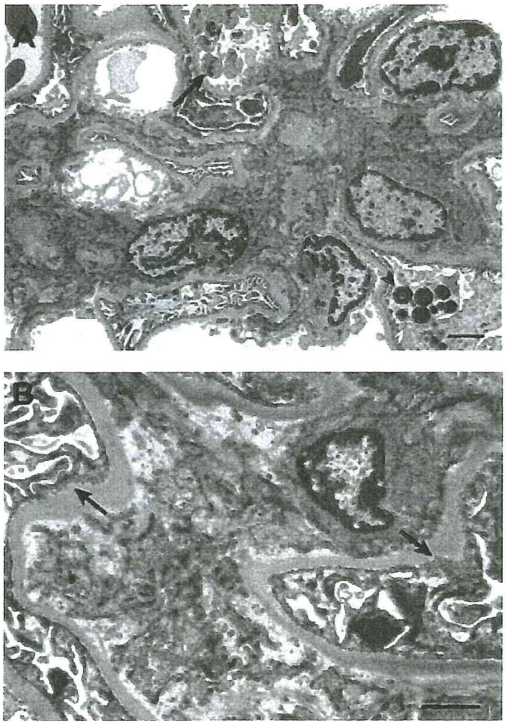

Fig. 5. Fine structures of glomerular lesions in the Hr^{krh}/Hr^{krh} rat. A: Proliferative lesions of mesangial matrices associated with significant dendritic projections from mesangial cells. Platelet aggregation was observed in a capillary loop (arrow). Intracellular hyaline droplets were significant in a podocyte (arrowhead). B: Foot process fusion (arrows) and a proliferative lesion of mesangial matrices that was not associated with dense deposits in mesangial regions and the glomerular basement membrane. Bar: 2 μm.

sociated with severe proteinuria. FGS is a descriptor for a pathological finding in the kidneys. When a nephritic range of proteinuria is observed, patients are diagnosed as having focal segmental glomerulosclerosis (FSGS). FSGS is classified by morphological variants including collapsed glomeruli, cellular proliferation, tip lesions, and diffuse mesangial proliferation [10]. The lesions that were observed in the F344-Hr^{krh} rat are characteristic of collapsed glomeruli associated with protein exudates in Bowman's capsule and may involve a collapsed variant of FSGS. Thus, the F344-Hr^{krh} rat may have potential as a model of nephritic FSGS.

FGS has not been reported for the APL or ALUNC family, and *Hr*-mutant mice, [2, 3, 7]. It is believed that FGS has a heterogeneous etiology and that it may manifest through multiple genetic factors [10]. The F344-Hr^{krh} rats were derived by employing ENU mutagenesis. The founder animals (G_1 generation) were expected to carry no more than four ENU-induced mutations in their CDS, if the CDS occupies 1% of the genome [16]. The F344-Hr^{krh} rats were mated by inbreeding without backcrossing to F344 rats to eliminate ENU-induced mutations other than the Hr^{krh} mutation. Thus, it is likely that the F344-Hr^{krh} rat may harbor mutation(s) that may play a role in the pathogenesis of FGS. FGS in Hr^{krh}/Hr^{krh} rats might be caused by unidentified mutation(s) that were induced by ENU or the combined effects of such mutation(s) with the Hr^{krh} mutation.

The Hr^{rh}/Hr^{rh} mouse has the nonsense mutation (R597X) [8] and develops hypergammaglobulinemia. The excess immunoglobulins that are produced due to this disease are deposited in the basement membranes of the skin, spleen, liver, and kidney, and antinuclear antibodies are produced. These symptoms appear in young mice and increase in severity with age [14]. Although the F344-Hr^{krh}/Hr^{krh} rat has a nonsense mutation (S413X), the mutation is not associated with an autoimmune disease or IgM, IgG, and C3 deposition in the kidneys (data not shown). Generally, pathological phenotypes that are associated with this disease are often influenced by a predisposed genetic background [18, 19]. Therefore, genes that are predisposed to causing autoimmune diseases in *rh/rh* mice may be absent in F344-Hr^{krh} rats. By replacing the genetic background of F344-Hr^{krh} with those of other rat strains, we might find autoimmune disease in Hr^{krh}/Hr^{krh} rats.

In summary, a novel rat mutant strain, F344-Hr^{krh}, was established that carries an *Hr* nonsense mutation (S413X). In addition to the hair loss phenotype, Hr^{krh} homozygous rats suffer from proteinuria and FGS. Therefore, F344-Hr^{krh} may have potential as a model of skin disease as well as nephritic FSGS.

Acknowledgments

This work was supported in part by Grants-in-aid for Scientific Research from the Japan Society for the Promotion of Science (21300153 to TK) and a Grant-in-aid for Cancer Research from the Ministry of Health, Labour

and Welfare. We are grateful to M. Yokoe, M. Terada, N. Takahira, and M. Sudo for their excellent technical assistance. Rat strain F344-*Hr*^{krh} (NBRP Rat No: 0471) is deposited in the National BioResource Project-Rat.

References

1. Ahearn, K., Akkouris, G., Berry, P.R., Chrissluis, R.R., Crooks, I.M., Dull, A.K., Grable, S., Jeruzal, J., Lanza, J., Lavoie, C., Maloney, R.A., Pitruzzello, M., Sharma, R., Stoklasek, T.A., Tweeddale, J., and King, T.R. 2002. The Charles River "hairless" rat mutation maps to chromosome 1: allelic with fuzzy and a likely orthologue of mouse frizzy. *J. Hered.* 93: 210–213.
2. Ahmad, W., Faiyaz ul Haque, M., Brancolini, V., Tsou, H.C., ul Haque, S., Lam, H., Aita, V.M., Owen, J., deBlaquiere, M., Frank, J., Cserhalmi-Friedman, P.B., Leask, A., McGrath, J.A., Peacocke, M., Ahmad, M., Ott, J., and Christiano, A.M. 1998. Alopecia universalis associated with a mutation in the human hairless gene. *Science* 279: 720–724.
3. Ahmad, W., Ratterree, M.S., Panteleyev, A.A., Aita, V.M., Sundberg, J.P., and Christiano, A.M. 2002. Atrichia with papular lesions resulting from mutations in the rhesus macaque (*Macaca mulatta*) hairless gene. *Lab. Anim.* 36: 61–67.
4. Ahmad, W., Zlotogorski, A., Panteleyev, A.A., Lam, H., Ahmad, M., ul Haque, M.F., Abdallah, H.M., Dragan, L., and Christiano, A.M. 1999. Genomic organization of the human hairless gene (*HR*) and identification of a mutation underlying congenital atrichia in an Arab Palestinian family. *Genomics* 56: 141–148.
5. Aitman, T.J., Critser, J.K., Cuppen, E., Dominiczak, A., Fernandez-Suarez, X.M., Flint, J., Gauguier, D., Geurts, A.M., Gould, M., Harris, P.C., Holmdahl, R., Hubner, N., Izsvak, Z., Jacob, H.J., Kuramoto, T., Kwitek, A.E., Marrone, A., Mashimo, T., Moreno, C., Mullins, J., Mullins, L., Olsson, T., Pravenec, M., Riley, L., Saar, K., Serikawa, T., Shull, J.D., Szpirer, C., Twigger, S.N., Voigt, B., and Worley, K. 2008. Progress and prospects in rat genetics: a community view. *Nat. Genet.* 40: 516–522.
6. Bazzi, H., Kljuic, A., Christiano, A.M., and Panteleyev, A.A. 2004. Intragenic deletion in the Desmoglein 4 gene underlies the skin phenotype in the Iffa Credo "hairless" rat. *Differentiation* 72: 450–464.
7. Bult, C.J., Eppig, J.T., Kadin, J.A., Richardson, J.E., and Blake, J.A. 2008. The Mouse Genome Database (MGD): mouse biology and model systems. *Nucleic Acids Res.* 36: D724–728.
8. Cachon-Gonzalez, M.B., San-Jose, I., Cano, A., Vega, J.A., Garcia, N., Freeman, T., Schimmang, T., and Stoye, J.P. 1999. The hairless gene of the mouse: relationship of phenotypic effects with expression profile and genotype. *Dev. Dyn.* 216: 113–126.
9. Cichon, S., Anker, M., Vogt, I.R., Rohleder, H., Putzstuck, M., Hillmer, A., Farooq, S.A., Al-Dhafri, K.S., Ahmad, M., Haque, S., Rietschel, M., Propping, P., Kruse, R., and Nothen, M.M. 1998. Cloning, genomic organization, alternative transcripts and mutational analysis of the gene responsible for autosomal recessive universal congenital alopecia. *Hum. Mol. Genet.* 7: 1671–1679.
10. Dagati, V. 1994. The many masks of focal segmental glomerulosclerosis. *Kid. Int.* 46: 1223–1241.
11. Friedman, J.M., Leibel, R.L., and Bahary, N. 1991. Molecular mapping of obesity genes. *Mamm. Genome* 1: 130–144.
12. Inazu, M. and Sakaguchi, T. 1984. Morphologic characteristics of the skin of bald mutant rats. *Lab. Anim. Sci.* 34: 584–587.
13. Ishii, Y., Tsutsui, S., Doi, K., and Itagaki, S. 1997. Hair follicles of young Wistar strain hairless rats: a histological study. *J. Anat.* 191: 99–106.
14. Kawaji, H., Tsukuda, R., and Nakaguchi, T. 1980. Immunopathology of rhino mouse, an autosomal recessive mutant with murine lupus-like disease. *Acta Pathol. Jpn.* 30: 515–530.
15. Kuramoto, T., Kitada, K., Inui, T., Sasaki, Y., Ito, K., Hase, T., Kawagachi, S., Ogawa, Y., Nakao, K., Barsh, G.S., Nagao, M., Ushijima, T., and Serikawa, T. 2001. Attractin/mahogany/zitter plays a critical role in myelination of the central nervous system. *Proc. Natl. Acad. Sci. U.S.A.* 98: 559–564.
16. Mashimo, T., Yanagihara, K., Tokuda, S., Voigt, B., Takizawa, A., Nakajima, R., Kato, M., Hirabayashi, M., Kuramoto, T., and Serikawa, T. 2008. An ENU-induced mutant archive for gene targeting in rats. *Nat. Genet.* 40: 514–515.
17. Nanashima, N., Akita, M., Yamada, T., Shimizu, T., Nakano, H., Fan, Y., and Tsuchida, S. 2008. The hairless phenotype of the Hirosaki hairless rat is due to the deletion of an 80-kb genomic DNA containing five basic keratin genes. *J. Biol. Chem.* 283: 16868–16875.
18. Nose, M. 2007. A proposal concept of a polygene network in systemic vasculitis: lessons from MRL mouse models. *Allergol. Int.* 56: 79–86.
19. Nose, M., Nishimura, M., and Kyogoku, M. 1989. Analysis of granulomatous arteritis in MRL/Mp autoimmune disease mice bearing lymphoproliferative genes. The use of mouse genetics to dissociate the development of arteritis and glomerulonephritis. *Am. J. Pathol.* 135: 271–280.
20. Panteleyev, A.A., Botchkareva, N.V., Sundberg, J.P., Christiano, A.M., and Paus, R. 1999. The role of the hairless (*hr*) gene in the regulation of hair follicle catagen transformation. *Am. J. Pathol.* 155: 159–171.
21. Serikawa, T., Mashimo, T., Takizawa, A., Okajima, R., Maedomari, N., Kumafuji, K., Takami, F., Neoda, Y., Otsuki, M., Nakanishi, S., Yamasaki, K., Voigt, B., and Kuramoto, T. 2009. National BioResource Project-Rat and related activities. *Exp. Anim.* 58: 333–341.
22. Sun, J., Silva, K.A., McElwee, K.J., King, L.E., and Sundberg, J.P. 2008. The C3H/HeJ mouse and DEBR rat models for alopecia areata: review of preclinical drug screening approaches and results. *Exp. Dermatol.* 17: 793–805.
23. Thompson, C.C., Sisk, J.M., and Beaudoin, G.M. 3rd. 2006. Hairless and Wnt signaling: allies in epithelial stem cell differentiation. *Cell Cycle* 5: 1913–1917.

OPEN ACCESS Freely available online PLoS GENETICS

A Mutation in the Gene Encoding Mitochondrial Mg^{2+} Channel MRS2 Results in Demyelination in the Rat

Takashi Kuramoto[1]*, Mitsuru Kuwamura[2], Satoko Tokuda[1,2], Takeshi Izawa[2], Yoshifumi Nakane[1], Kazuhiro Kitada[1,3], Masaharu Akao[4], Jean-Louis Guénet[5], Tadao Serikawa[1]

1 Institute of Laboratory Animals, Graduate School of Medicine, Kyoto University, Kyoto, Japan, **2** Laboratory of Veterinary Pathology, Osaka Prefecture University, Osaka, Japan, **3** Laboratory of Mammalian Genetics, Genome Dynamics Research Center, Graduate School of Science, Hokkaido University, Sapporo, Japan, **4** Department of Cardiovascular Medicine, Graduate School of Medicine, Kyoto University, Kyoto, Japan, **5** Département de Biologie du Développement, Institut Pasteur, Paris, France

Abstract

The rat demyelination (*dmy*) mutation serves as a unique model system to investigate the maintenance of myelin, because it provokes severe myelin breakdown in the central nervous system (CNS) after normal postnatal completion of myelination. Here, we report the molecular characterization of this mutation and discuss the possible pathomechanisms underlying demyelination. By positional cloning, we found that a G-to-A transition, 177 bp downstream of exon 3 of the *Mrs2* (MRS2 magnesium homeostasis factor (*Saccharomyces cerevisiae*)) gene, generated a novel splice acceptor site which resulted in functional inactivation of the mutant allele. Transgenic rescue with wild-type *Mrs2*-cDNA validated our findings. *Mrs2* encodes an essential component of the major Mg^{2+} influx system in mitochondria of yeast as well as human cells. We showed that the *dmy/dmy* rats have major mitochondrial deficits with a markedly elevated lactic acid concentration in the cerebrospinal fluid, a 60% reduction in ATP, and increased numbers of mitochondria in the swollen cytoplasm of oligodendrocytes. MRS2-GFP recombinant BAC transgenic rats showed that MRS2 was dominantly expressed in neurons rather than oligodendrocytes and was ultrastructurally observed in the inner membrane of mitochondria. Our observations led to the conclusion that *dmy/dmy* rats suffer from a mitochondrial disease and that the maintenance of myelin has a different mechanism from its initial production. They also established that Mg^{2+} homeostasis in CNS mitochondria is essential for the maintenance of myelin.

Citation: Kuramoto T, Kuwamura M, Tokuda S, Izawa T, Nakane Y, et al. (2011) A Mutation in the Gene Encoding Mitochondrial Mg^{2+} Channel MRS2 Results in Demyelination in the Rat. PLoS Genet 7(1): e1001262. doi:10.1371/journal.pgen.1001262

Editor: Gregory S. Barsh, Stanford University, United States of America

Received June 5, 2010; **Accepted** November 29, 2010; **Published** January 6, 2011

Copyright: © 2011 Kuramoto et al. This is an open-access article distributed under the terms of the Creative Commons Attribution License, which permits unrestricted use, distribution, and reproduction in any medium, provided the original author and source are credited.

Funding: This work was supported by grants-in-aid for Scientific Research from the Japan Society for the Promotion of Science [21300153 to TK] and a grant-in-aid for Cancer Research from the Ministry of Health, Labour, and Welfare. The funders had no role in study design, data collection and analysis, decision to publish, or preparation of the manuscript.

Competing Interests: The authors have declared that no competing interests exist.

* E-mail: tkuramot@anim.med.kyoto-u.ac.jp

Introduction

Myelin is an essential component of the nervous tissue of higher vertebrates. It acts as a natural insulator of axonal segments allowing, at the same time, the maintenance of axonal integrity and the fast conduction of action potentials. It also reduces ionic currents across the axonal membrane and stabilizes the extracellular milieu within rapidly-firing axon bundles.

In the central nervous system (CNS), myelin is produced by oligodendrocytes, while in the peripheral nervous system (PNS), this function is achieved by Schwann cells. Myelination is completed within a relatively short period of time during mammalian development and requires a high rate of production and transport of different kinds of molecules, mostly proteins and lipids. In adult life, myelin is constantly remodeled and the maintenance of functional myelin sheaths requires a careful balance of *de novo* synthesis and turnover. It is quite clear that any event generating an imbalance in the myelination or remyelination process has the greatest chance of inducing dys- or demyelination of either the central or peripheral nervous system.

Our knowledge of the myelination process has benefited from careful observations conducted on human patients affected by one of the many defects of myelination or myelin turnover. It has also benefited from researches carried out on animal models, mostly mutant mice and rats, including those that have been induced by transgenesis or genetic engineering in ES cell lines [1,2]. Some of these models have even allowed therapies to be developed in a preclinical setting [3]. Unfortunately, only a small number of the many genes that are directly or indirectly involved in the myelination process have been identified and only a few of these genes have been functionally annotated, for example, by the characterization of one or more mutant alleles. For this reason, any new mutation occurring spontaneously or after mutagenesis is of potential interest for unraveling the molecular mechanisms involved in myelin assembly.

In an earlier paper we reported the discovery and pathology of a rat mutation designated *demyelination* (symbol *dmy*), which is characterized by severe and progressive myelin breakdown in the CNS. We mapped the locus responsible for this myelin disorder to rat chromosome (Chr) 17, very close to the prolactin (*Prl*) locus, in a region homologous to human Chr 6p21.1-22.3 and mouse Chr 13 [4,5]. Based on its pathological features, as well as its genetic localization, this demyelination syndrome appeared to be unique, with no homologue so far reported in any other mammalian species, including humans.

Author Summary

The myelin sheath that surrounds the axon of a neuron acts as a biological insulator. Its major function is to increase the speed at which impulses propagate along myelinated fibers in the central nervous system, as well as the peripheral nervous system. Alterations or damage affecting this structure (demyelination) result in the disruption of signals between the brain and other parts of the body. In the rat, mutations producing demyelination have been frequently identified and characterized and have contributed to a better understanding of the genetics of myelin development, physiology, and pathology. This paper reports the molecular characterization of a recessive allele responsible for the progressive disruption of myelin that was initially observed in mutant rats, previously named demyelination (*dmy*). This mutation generates an additional splicing acceptor site in an intron of the mitochondrial Mg^{2+} transporter gene (*Mrs2*), resulting in the insertion of a 83-bp genomic DNA segment into the *Mrs2* transcript and complete functional inactivation of the mutant allele. We firstly defined the biological function of MRS2 in mammals and demonstrated the crucial and unexpected role of MRS2 in myelin physiology. Our findings might be helpful in the development of new therapeutic strategies for demyelinating syndromes.

In this report we demonstrate that the causative gene (*Mrs2*) encodes a protein that is an essential component of the major electrophoretic Mg^{2+} influx system in mitochondria [6]. This gene has orthologues in other organisms, including lower eukaryotes and plants [7,8]. The protein shares many of the properties of bacterial CorA and yeast Alr1 proteins but its specific involvement in the myelination process was not known or even suspected.

Results

dmy/dmy rats exhibit a phenotype with typical demyelination

The pathology of homozygous *dmy/dmy* rats has been reported in detail previously [4]. Mutant rats exhibit no significant differences from their control littermates until 4 weeks of age. From 5 weeks on, flaccidity of the hind limbs becomes noticeable and evolves towards complete paralysis around 7–8 weeks of age. Progressive demyelination is observed in several parts of the CNS (Figure 1), namely the corpus callosum, the capsula interna, the striatum and the cerebellar peduncle, with major effects on the ventral and lateral parts of the spinal cord. Astrogliosis, which is a major feature of myelin disorder, is observed in demyelinated areas but motor neurons remain normal and there is no sign of associated inflammation in the white matter. The *dmy* mutation can then be regarded as a mutation affecting the maintenance and turnover of myelin rather than its initial production: this is typical demyelination [9].

The *dmy* syndrome is associated with a mutation in a splicing site of *Mrs2*, a gene encoding a mitochondrial Mg^{2+} channel

Out of 687 *dmy/dmy* mutant rats, collected from the 3,252 offspring of an intercross segregating for the *dmy* mutation, 23 individuals were found to carry a recombinant haplotype between the two loci that were used for the initial genetic mapping, namely; *Prl* (prolactin) and *Hh1tts* (testis-specific histone, H1t). Further investigation of these animals, using three novel informative SSLP markers, allowed us to narrow the genetic interval containing *dmy* down to 0.22 cM, between markers *D17Kur17* and *D17Got45*. Within this critical section, we found no recombination between the *dmy* locus and either *Aldh5a1* (aldhehyde dehydrogenase family 5, subfamily A1) or *Mrs2* (mitochondrial 118 RNA splicing2) loci, among $687 \times 2 = 1{,}374$ meioses. The rat genome databases revealed that *D17Kur17* and *D17Got45* were at position 46.78-Mb and 47.26-Mb, respectively, on rat Chr 17, yielding a physical size of 0.48 Mb of DNA for the interval containing the *dmy* locus. This stretch of DNA contained 6 genes (Figure 2A).

Analysis by RT-PCR of the transcription products of these 6 genes revealed that the cDNA transcribed from the *Mrs2* gene was larger in *dmy/dmy* mutants than in the controls (Figure 2B). After sequencing, we found that the larger size of the *dmy* cDNA was due to the insertion of an 83 bp intronic sequence between exons 3 and 4. Comparison of the two genomic sequences revealed a G-to-A transition, 177 bp downstream of the end of exon 3 (Figure 2C, Figure S1), generating a novel splice acceptor site, which accounted for the addition of the 83bp stretch of intronic sequence to the mutant transcript. In addition, while the *Mrs2* gene normally encodes a 434 amino-acid protein, the intronic insertion leads to a shorter protein (106 amino acids) due to the occurrence of a stop codon as a consequence of frame shifting within the novel pseudo-exon X. The new protein consisted of the first 91 amino acids of normal (wild-type) MRS2 protein followed by an additional 15 amino acids transcribed from the intronic stretch (Figure 2D) [10]. No nucleotide alteration was observed between normal and mutant haplotypes in the cDNA transcribed from the other 5 genes (*Vmp*, *Dcdc2*, *Gpld1*, *Aldh5a1*, and *KIAA0319*). These findings strongly suggested that the G-to-A mutation in intron 3 of *Mrs2* in *dmy/dmy* rats was very likely causative of the neurological phenotype.

dmy/dmy rats exhibit morphological and biochemical features characteristic of mitochondrial deficiencies

The MRS2 protein functions as a major transporter protein (Mg^{2+}, Ni^{2+} and Co^{2+}) in yeast as well as in human cells [10,11]. When this protein is functionally defective this leads to the "petite" phenotype in yeast and to cell death in human HEK 293 cells [11,12]. Because mitochondrial diseases in mammals are often accompanied by elevated lactic acid, reduced ATP, increased cytochrome oxidase (COX) activity, and the morphological alteration of mitochondria [13–15], we measured lactic acid levels and ATP contents in the CNS and performed morphological analyses of the CNS of *dmy/dmy* rats.

Lactic acid concentration in the cerebrospinal fluids was significantly elevated in *dmy/dmy* rats when compared with normal littermates: 126 ± 43.7 mg/dL vs 25 ± 9.6 mg/dL (average $\pm$ SD), $P<0.002$ (Figure 3A). The ATP concentration was markedly reduced in *dmy/dmy* rats: 265 ± 79 μM/mg vs 99 ± 46 μM/mg (average $\pm$ SD), $P<0.005$ (Figure 3B). In the affected *dmy/dmy* rats, swollen oligodendrocytes were often observed in the white matter, showing the increased COX reaction products (Figure 3C). Ultrastructurally, their cytoplasm contained many mitochondria and Golgi apparatus-like membrane structures (Figure 3D). These findings indicated that the mitochondria of *dmy/dmy* rats were functionally defective.

Rescue of *dmy/dmy* mutant phenotypes by transgenic complementation

To ascertain that the molecular defect (*i.e.* G-to-A transition) observed in the *dmy* mutant haplotype was causative of the abnormal phenotype observed in *dmy/dmy* rats, we attempted to rescue the mutant phenotype by transgenic complementation. We

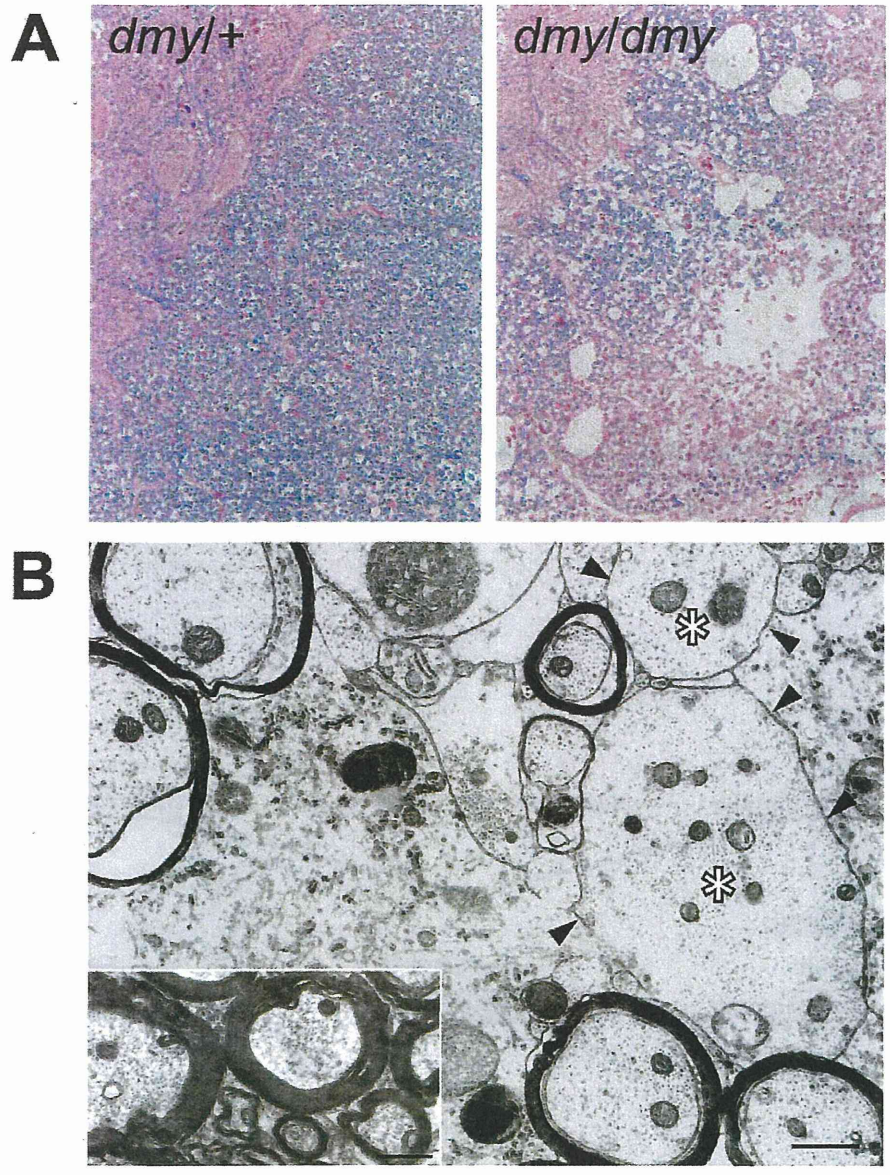

Figure 1. Demyelination in *dmy/dmy* rats. A. Histopathology of the cervical part of the spinal cord of *dmy/+* (left) and *dmy/dmy* (right) rats aged 10 weeks. Luxol fast blue-HE staining. Original magnification: ×100. B. Electron microscopy of the cervical part of spinal cord of *dmy/dmy* rats (10 weeks). Naked axons with demyelination (arrowheads) are indicated by asterisks. Inset: control image of the spinal cord from the age-matched wild type rat. Axons are normally myelinated. Bar = 1 μm.
doi:10.1371/journal.pgen.1001262.g001

established two independent WTC.DMY-*dmy* lines, expressing each *Mrs2* wild-type cDNA under the control of a cytomegalovirus (CMV) promoter (Figure S2A), and found that all *dmy/dmy* transgenic rats exhibited a completely normal phenotype, with no paralysis of the hind limbs. Histopathological analyses demonstrated that both transgenic lines no longer exhibited any sign of demyelination of the CNS (Figure S2B). In addition, lactic acid levels of the cerebrospinal fluid of transgenic *dmy/dmy* rats had returned to the normal range (Figure S2C). Electron microscopic observations revealed that mitochondria of the oligodendrocytes in transgenic rats were normal in their morphology and number (Figure S2D). These findings confirmed that the molecular changes reported above and observed in the *Mrs2* gene were indeed causative of the *dmy*-mutant phenotypes. For this reason we decided that the symbol of the mutant allele should, from now on, be changed to $Mrs2^{dmy}$.

MRS2-GFP recombinant protein is expressed in the mitochondria

To characterize the tissues and cell types expressing MRS2 as well as the subcellular localization of this protein in the CNS, we generated a strain of rats transgenic for a recombinant MRS2-GFP BAC clone. These transgenic rats were expected to express recombinant protein under the control of the endogenous, normal *Mrs2* promoter. We found that cytoplasmic dot-like MRS2-GFP

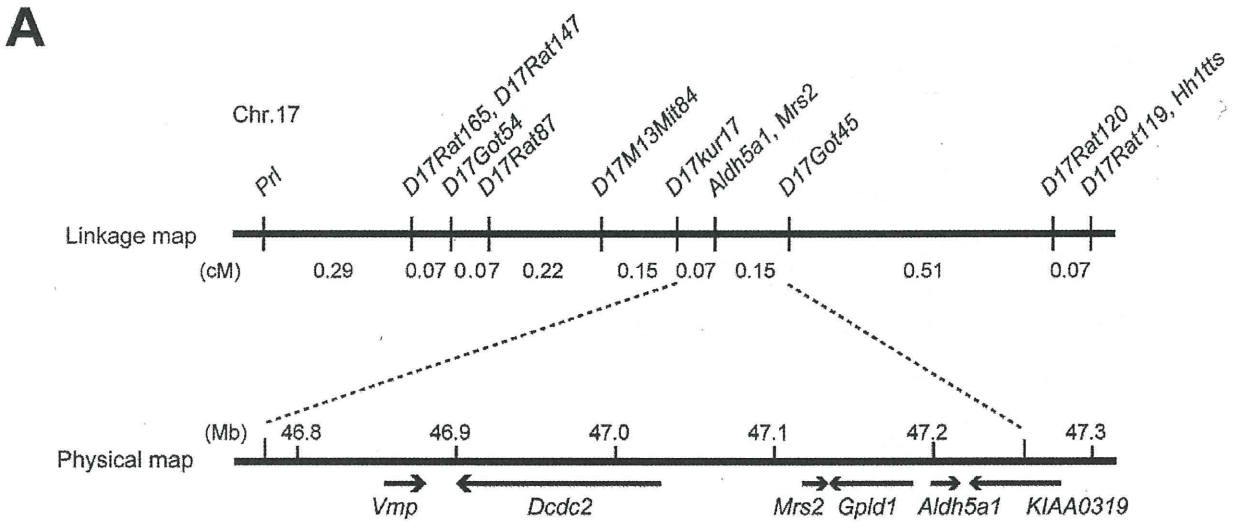
A
Chr.17
Prl
D17Rat165, D17Rat147
D17Got54
D17Rat87
D17M13Mit84
D17kur17
Aldh5a1, Mrs2
D17Got45
D17Rat120
D17Rat119, Hh1tis
Linkage map
(cM)
0.29
0.07
0.07
0.22
0.15
0.07
0.15
0.51
0.07
(Mb)
46.8
46.9
47.0
47.1
47.2
47.3
Physical map
Vmp
Dcdc2
Mrs2
Gpld1
Aldh5a1
KIAA0319


B
M
+/+
dmy/dmy

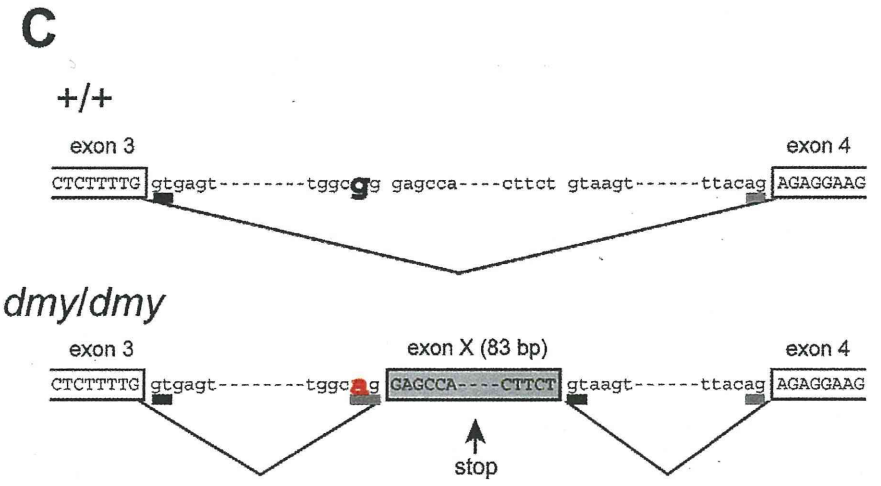
C
+/+
exon 3
exon 4
CTCTTTTG gtgagt--------tggcgg gagcca----cttct gtaagt------ttacag AGAGGAAG
dmy/dmy
exon 3
exon X (83 bp)
exon 4
CTCTTTTG gtgagt--------tggcag GAGCCA----CTTCT gtaagt------ttacag AGAGGAAG
stop

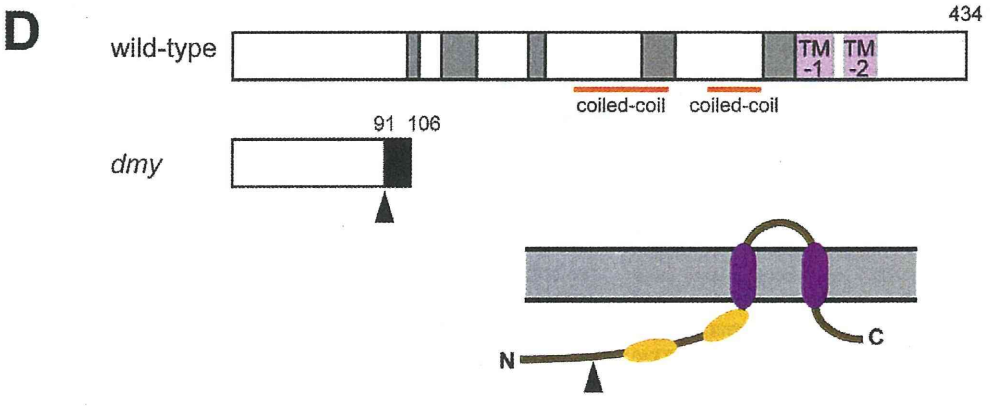
D
wild-type
434
TM -1
TM -2
coiled-coil
coiled-coil
dmy
91 106
N
C

Figure 2. Positional cloning of the *dmy* mutation. A. The *dmy* locus was localized within a 0.22-cM region of chromosome 17 between *D17Kur17* and *D17Got45* and no recombination was observed with SSLP markers designed from *Aldh5a1* and *Mrs2* genomic sequences in 1,374 informative meioses. Within the 0.48-Mb physical interval between *D17Kur17* and *D17Got45*, harboring the *dmy* locus, 6 genes: *Vmp* (vesicular membrane protein p24), *Dcdc2* (doublecortin domain containing 2), *Mrs2* (MRS2 magnesium homeostasis factor (*S. cerevisiae*), *Gpld1* (glycosylphosphatidylinositol specific phospholipase D1), *Aldh5a1* (aldehyde dehydrogenase family 5, subfamily A1), and *KIAA0319*, were previously mapped. B. A larger RT-PCR product was obtained when amplifying the 5′ region of *Mrs2* cDNAs from *dmy/dmy* rats with a primer set of rMrs2I-3&4 (5′-TGTACTGATCTACCCGAGTTCC-3′ and 5′-TCTGGAGTTATCACAGCCTTCA-3′). M: molecular marker, ΦX174-*Hae*III digest. C. Upper: Genomic organization in the vicinity of intron 3 of the *Mrs2* wild-type allele. Lower: Genomic rearrangements in the same intron 3 of the $Mrs2^{dmy}$ mutant allele. In the $Mrs2^{dmy}$ mutant allele, a novel splice acceptor site was generated as a consequence of a G-to-A transition at 177 bp downstream of the end of exon 3. An 83-bp genomic sequence (boxed in gray), downstream of the recently generated acceptor site (tggcag), is then inserted into the *Mrs2* mutant transcript. This sequence contains a premature stop codon (vertical arrow), which truncates the protein almost immediately downstream of exon 3. D. Schematic representations of the wild-type and *dmy* MRS2 proteins. Conserved amino acid residues and transmembrane domains are indicated by grey and purple boxes, respectively. Coiled-coil regions are indicated by horizontal orange lines. The position of the *dmy* mutation is indicated by an arrowhead, and the additional 15 residues (GATWTPRILEECLES), indicated by a black box, are deduced to be added subsequently. Bottom: Schematic representation of the topology of MRS2. Purple: transmembrane domains, Orange: coiled-coil regions. The position of the *dmy* mutation is indicated by an arrowhead.
doi:10.1371/journal.pgen.1001262.g002

signals were observed in neurons throughout the CNS. To a lesser extent, astrocytes and oligodendrocytes also exhibited occasional expression of MRS2 (Figure S3). Confocal microscopy demonstrated that MRS2 is located in the mitochondria (Figure 4A–4C). Moreover, immunoelectron microsopic examinations with anti-GFP antibody revealed that MRS2 is localized in the inner membrane of the mitochondria (Figure 4D). MRS2 expression was also observed in the myocardium, liver, testis and skeletal muscles (Figure S4).

Microglia activation and high expression of inflammatory cytokines were observed in $Mrs2^{dmy}/Mrs2^{dmy}$ rats

Microglial activation, characterized by cellular hypertrophy, has been reported in various dysmyelinating and demyelinating pathologies. To assess microglial activation, we performed immunohistochemistry for IBA1, a specific marker of microglia. In $Mrs2^{dmy}/Mrs2^{dmy}$ rats, prolonged activation of microglia was prominently observed at 6–7 weeks of age (Figure 5A and 5B), the stage at which clinical symptoms such as flaccid paralysis were commonly observed. Expression levels of proinflammatory cytokines, such as *Il1b* and *Il6*, were also significantly higher in $Mrs2^{dmy}/Mrs2^{dmy}$ rats than in wild-type littermates at 6 weeks of age (Figure 5C).

Discussion

Characterization, by positional cloning, of the molecular defect responsible for the demyelinating phenotype observed in adult *dmy/dmy* rats led us to incriminate a mutation in the *Mrs2* gene. No mutant allele before $Mrs2^{dmy}$, which we report here, has ever been reported at this locus in any mammalian species.

Mrs2 encodes an inner membrane Mg^{2+} channel in mitochondria and belongs to a family with orthologous copies in a wide range of species [10,12]. *Mrs2* was originally identified in yeast, and orthologous copies of this gene have been identified in a variety of organisms, including bacteria (CorA), fungi (Alr1), and plants (AtMrs2). All proteins in the family have the same substrate selectivity: they transport Mg^{2+}, Co^{2+} and some other divalent cations across the mitochondrial membrane. Even if these proteins exhibit relatively low sequence similarities, they all have a few important domains at the same relative position and can functionally complement each other over a wide range of phylogenetic distances [16,17]. In mammals, the normal protein MRS2 has two universally conserved transmembrane domains (TMs) and a conserved Gly-Met-Asn (GMN) motif close to the first TM domain that forms part of the pore and is essential for Mg^{2+} transport [18] (Figure 2D, Figure S5). As we demonstrated, the protein is truncated in *dmy/dmy* mutant rats, having lost both of its essential domains and accordingly its function of an Mg^{2+} transmembrane transporter. In other words, $Mrs2^{dmy}$ is a null allele, which is totally consistent with its recessive allelic interaction.

An MRS2 is a major transport for Mg^{2+} uptake into mitochondria, its function would be expected to be important, if not essential, for the maintenance of respiratory complex I and accordingly for cell viability [6,11]. This assumption was supported by the analysis of MRS2 knock-down, mediated by shRNA in a human HEK-293 cell line, which resulted in a series of physiological changes ranging from transient reduction of Mg^{2+} uptake to the complete loss of mitochondrial respiratory complex I, with decreased mitochondrial membrane potential and cell death, depending on the duration of knock-down treatment [11]. However, if we consider the phenotype of our mutant rat, which is apparently limited to the myelination process with a rather long lifespan, the role of MRS2 in the maintenance of cell integrity should be reconsidered.

Considering the pathological features that appear to be characteristics of the $Mrs2^{dmy}$ allele on the one hand, and MRS2-specific functions, as described above on the other, it is logical to consider that the demyelinating syndrome in mutant rats results from a mitochondrial disease. This assertion is supported by the observation of an elevated rate of lactic acid in the cerebrospinal fluid, reduced ATP in the brain, increased COX activity, and the morphological alteration of mitochondria, which is generally considered a major characteristic of mitochondrial diseases [13–15]. An increase in mitochondria is characteristic of cells with reduced respiratory capacity [19]. The association of mitochondrial dysfunction with demyelination (or leukodystrophy) has been already reported in Leigh syndrome and mitochondrial DNA depletion syndrome [20–23]. The tissues most frequently affected in these mitochondrial diseases are the cerebrum, peripheral nerves, and skeletal muscles, presumably because cells of these tissues require more energy than any other cells in the body. Unfortunately, the detailed pathophysiological mechanism(s) leading to demyelination in these diseases has not yet been unraveled. We consider that our mutant rat could be an interesting tool for investigating this matter.

Mitochondrial dysfunction has also been observed in multiple sclerosis (MS), one of the most common demyelination diseases, but here again many aspects of the pathophysiology require further investigation [24,25]. This difficulty of linking gene functions with a specific syndrome is not so surprising if we consider that, according to the most recent estimates, there may be as many as 1,500 nuclear-encoded mitochondrial proteins [26] and that less than half have been identified with experimental support. Clearly, a complete protein inventory of this organelle